TsAGI Science Journal, 45(3–4), 273–292 (2014)

SIMULATION OF PERIODIC VORTICAL STRUCTURES IN THE AIRFOIL WAKE

P. A. Baranov,[1] S. V. Guvernyuk,[2] S. A. Isaev,[3] A. G. Soudakov,[1] & A. E. Usachov[4,*]

[1]Battery Company "RIGEL," 38, Professor Popov Str., St. Petersburg, 197376 Russia; [2]Institute of Mechanics, Lomonosov Moscow State University, 1, Michurinskii Prospekt, Moscow, 119192 Russia; [3]Saint Petersburg State University of Civil Aviation, 38 Pilotov Str., St. Petersburg, 196210 Russia; [4]Central Aerohydrodynamic Institute (TsAGI), 1 Zhukovsky Str., Zhukovsky, Moscow Region, 140180 Russia

*Address all correspondence to A. E. Usachov E-mail: usachov_a@mtu-net.ru

Parametrical calculations of an unsteady flow around a NACA 0012 airfoil at a fixed Reynolds number of 40,000 are performed using several multi-block overlapping grids of different scales and densities, which cover settlement areas of various extents, including the near and far wakes. The solutions found by Menter's shear stress transport model, the Spalart–Allmaras vortex viscosity transport model, and the method of vortical domains, are compared with available estimated and experimental data. Verification of the two-dimensional model is performed by comparison of the numerical predictions for a cross flow over a thick plate with Igarashi's experimental data.

KEY WORDS: *numerical simulation, turbulence, airfoil, procedure of pressure correction, multi-block computing technologies, VP2/3 software package*

1. INTRODUCTION

Unsteady vortical fields are a source of acoustic disturbances. Periodical hydrodynamic processes of large vortex structure generation and propagation in the near- and far-field turbulent wakes of the NACA 0012 airfoil at angle of attack from 0 to 180° are considered in the present paper.

The problem regarding the flow over airfoils still attracts the attention of aerodynamic specialists. Interest in this problem has recently increased due to the numerical simulation of transonic unsteady flows [1, 2] and experiments aimed at studying the possibilities of flow control using blowing out of jets [3].

It is known that numerical solutions of the two-dimensional (2D) unsteady Reynolds averaged Navier–Stokes (URANS) equations supplemented with semi-empirical turbulence models differ quantitatively from the theoretical and experimental evaluations of the averaged integral characteristics of the NACA 0012 airfoil given in Refs. [4, 5]. This fact leads to the conclusion in Ref. [6] that the Reynolds approach is unacceptable for modeling unsteady separation flows and that an alternative approach based on a model of separated vortices has advantages in solving such problems. However, the 2D URANS approach is quite acceptable for modeling unsteady flow over a circular cylinder in sub/supercritical regimes [7–10] and also in the calculations implemented for airfoil NACA 0015 [11]. To resolve the situation, a detailed calculation of unsteady separated flows over airfoil NACA 0012 at a fixed Reynolds number of 40,000 is implemented in the present paper using different grids combined with multi-block computational technologies [12, 13], and the results found using several differential-type semi-empirical models are compared with the aforementioned experimental evaluations. The applicability of the 2D approach to the description of the turbulent separated flows is evaluated through a comparison of the obtained numerical predictions with the data from the Igarashi physical experiment for turbulent flow over a normal-to-airstream thick plate [14].

2. OBJECTIVE OF THE INVESTIGATION

Airfoil NACA 0012 is a classic symmetrical airfoil with an analytical statement of contour points [15]. Chord length L is a linear scale for transformation to dimensionless variables. The problem is solved in the wind coordinate system (x, y) with the reference point being in the middle of the chord and the x-axis being co-directed with the free stream. The inclination of the airfoil chord with respect to free-stream velocity U is specified by an angle of attack α. The problem of incompressible viscous fluid flow over airfoil NACA 0012 is solved in the rectangular calculation domain with the bounds being sufficiently far from the airfoil and the inlet bound being perpendicular to velocity U. The airfoil, moving with velocity U, is suddenly stopped in the initial time moment, and thereafter a process of stage formation of a vortex flow depending on the Reynolds number and determined by U, L, and the kinematic viscosity of the medium is developed (see, in particular, Ref. [12]).

An approach based on application of multi-block grids obtained by superimposing with intersections a priori introduced grids of simple topology (close to orthogonal) of different types and scales is developed in the present study. This approach is opposite to approaches based on mono-block grids or unstructured meshes, which for example are given in Ref. [6]. Each grid represents the corresponding element of a hydrodynamic structure of the airfoil flow. In Fig. 1(a), the outer Cartesian grid A is in agreement with the calculation domain bounds located sufficiently far (several hundred chords) from the airfoil [which is not distinguished in the scale in Fig. 1(a)]. In Fig. 1(b), the unsteady far-field wake behind the airfoil is represented in detail on the inner Cartesian grid B. A sufficiently fine cylindrical grid matched with the airfoil surface represents comparatively thin boundary and shear layers. Figure 1(c) shows curved grid C superimposed on Cartesian grids A and B at different densities.

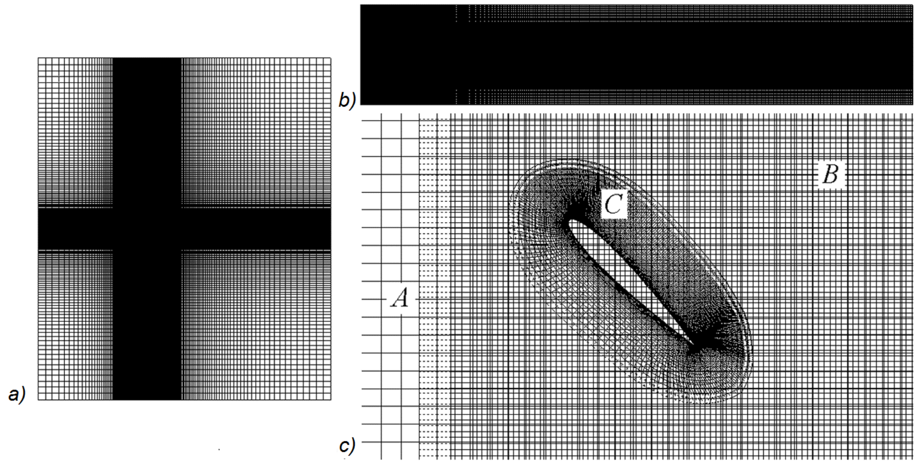

FIG. 1: Fragments of the multi-block grid: (a) outer Cartesian grid A; (b) internal Cartesian grid B, representing the far wake representation; (c) Cartesian grids A and B and cylindrical grid C superimposed in the airfoil area at a 45° angle of attack

An important methodological stage of the present numerical study is a comparative analysis of the results obtained using different differential semi-empirical models of turbulence (namely, one- and two- parametrical models). Along with the conventional Menter shear stress transfer (MSST) model [16], the modified Smirnov–Menter (SM) MSST model is applied, which takes into account a streamline curvature effect on the turbulence characteristics [17]. The one-equation turbulence Spalart–Allmaras (SA) model of vortex viscosity transfer is also used for comparison purposes [18].

The viscous vortex domain method (VVDM) [19], which is a meshless technique for solving the Navier–Stokes equations, is used along with grid numerical simulation techniques. Within this approach, there are no limitations to the calculation domain dimensions, and the resolution of the vortex structures is determined only with a specified initial airfoil discretization level. Such a complex approach to the simulation of unsteady flow over airfoil used to represent the airfoil far-field vortex wake.

Maintaining a starting vortex inside the calculation domain, which is especially intensive at high angles of attack, has great methodological importance. This fact determined the selected large dimensions of the calculation domain. The solving time is selected such that almost the whole vortex wake, including starting vortex, is inside grid A.

Fixing the Reynolds number in the calculations is not connected to any fundamental methodological limitations or to a desire to save computer power. The main reason is the necessity of a thorough handling of a huge amount of the information on unsteady processes of flow over the airfoil. Nevertheless, the near-wall step requirements are significantly less for $Re = 4 \times 10^4$.

As mentioned previously, handling of the unsteady flow characteristic calculation results is a special problem, which is not only connected to significant data. The approach, which relies on obtaining quasi-periodic regimes of airfoil flow characteristics, was used previously for a cylinder in [8–11] and is further developed in the present paper. Unsteady flow calculations usually lead to chaotic oscillation processes, which are handled using statistical methods. Characteristic variations are observed during an integral parameter oscillation period (for example, lift force). The processes are averaged over this period. A study of the solution behavior obtained within this time interval yields a detailed analysis of the unsteady flow regime with emphasis on the dynamics of vortex structures.

3. PROBLEM STATEMENT AND SOLVING TECHNIQUE

The problem of turbulent unsteady incompressible viscous fluid flow over an airfoil at an angle of attack is solved in the rectangular calculation domain with fixed input conditions. The scale dimensions are inlet flow velocity U and chord length L. The longitudinal flow velocity is $u = 1$; the transversal component is $v = 0$; the turbulence degree is 1%, which corresponds to the wind tunnel test section turbulence; and the turbulence scale is 1. The conditions for continuing the solution (soft boundary conditions) are specified by the outlet flow boundaries. The no-slip boundary condition is specified on the airfoil surface. The near-wall turbulence characteristics are calculated according to the methodology [13].

The URANS equations are solved using the pressure correction technique, which is based on the physical processes splitting concept and is related to replacement of the continuity equation by the equation for pressure correction (the SIMPLEC method). As in the steady case, the unsteady Reynolds approach for describing turbulence helps in obtaining the averaged flow and describing the velocity pulsation components with the introduced turbulent characteristics. The averaged flow in this case can vary with time.

As mentioned previously, a periodic solution to the problem with cyclic variation of the integral characteristics—in particular, the airfoil lift force—is sought. Similar to Refs. [12, 13], the generalized transport equation is rewritten in increments of dependent variables with the explicit part being discretized by high-order approximation schemes (not lower than the second order). Leonard quadratic upstream interpolation [20] is used for the convective terms of the momentum equation, the total variation diminishing (TVD) scheme [21] is used for the convective terms of the turbulence characteristics equations, and the central difference scheme is used for diffusive terms. The implicit part is represented by an upstream one-side difference scheme. Global iterations are used to find solution at each step [13]. The use of centered grids, in which the dependent variables are located in the centers of calculation cells, leads to the necessity of making the pressure field more monotone by using the Rhie–Chow correction with the multiplier, selected from the tests [12, 13] to be equal to 0.1. The calculations are implemented using multi-block grids (see, for example, Fig. 1). The external grid is constructed in a domain with dimensions of 300×200, with the reference point being distant from the inlet boundary by the 100 airfoil chords. The cells are clustered as long as the distance from the airfoil decreases. The minimal step of the external grid equals 0.1. The number of nodes is 672×201. The internal grid is close to uniform with the step of both coordinates being equal to 0.03; it contains 633 × 164 cells and is extended to approximately 60 airfoil chords. The cylindrical grid is matched with the airfoil. The grid step in the vicinity of the airfoil leading edge is 0.001, and the grid step in the vicinity of the trailing edge is 0.001 (the trailing edge radius is 0.002). The step in the airfoil middle part is 0.01. The near-wall step is 8×10^{-5}. The grid contains 329 × 62 cells. The time step is equal to 0.01.

4. METHODOLOGICAL STUDY, VERIFICATION, AND ANALYSIS OF INTEGRAL FORCE CHARACTERISTICS

The performed series of calculations of the flow over the airfoil, where the angle of attack was varied from 15 to 150°, is characterized by a regime of self-induced oscillations with periodical variation of error and integral streamwise and lateral loads, as demonstrated in Fig. 2 for $\alpha = 60$ and 90°. An initial phase of the flow/airfoil interaction, which is extended at 10–20 dimensionless time units, is characterized by increased pulsating loads, which decrease as long as the wake develops, similar to the case for turbulent flow over a circular cylinder [12, 13].

The analysis of the behavior of lateral loads on a self-induced oscillation regime of the airfoil flow enabled distinguishing the regions of their periodical variation (Figs. 3 and 4). In separate cases (at 135 and 150° angles of attack), we have to consider doubled regions. In order to compare the dependences of integral parameters $X(t)$ and $Y(t)$ in the regions of their periodical variation, we introduce reduced time t^*, which is counted from the moment the minimum Y value is reached.

A comparison of dependences $X\left(t^*\right)$ and $Y\left(t^*\right)$, shown in Fig. 3, also has methodological characteristic because the results were obtained in the calculation domains that differed significantly in their dimensions, namely, in the 40 × 20 and 300 × 200 domains. As mentioned previously, for large calculation domains almost the whole vortex wake, including the starting vortex, is in the domain, and for the smaller domains the starting vortex abandons the domain. A periodical character of the vortex formation process is difficult to reveal in smaller-dimension domains, and this fact influences the calculation of the flow over the airfoil at high angles of attack (higher than 60°). At the same time, up to an angle of attack of 60° (see Fig. 3), agreement between the results of the calculation of the unsteady integral characteristics of the NACA 0012 airfoil are sufficiently satisfactory (see Fig. 3, curves 7, 11 and 8, 12).

As long as the angle of attack increases, the periodical dependences of the integral parameters versus time become more different from the sinusoidal one, which is typical for small angles of attack (until 25° and higher than 155°).

The conclusion that the application of 2D URANS in the calculation of airfoil flow is unacceptable for high angles of attack was made in Ref. [6] based on misalignment of numerical predictions obtained with the use of the MSST model [22], SA model ($Re = 10^5$), and Hoerner data [4]. The evaluations [5] can also be added to the aforementioned results (Fig. 5). At the same time, the results obtained for $Re = 4 \times 10^4$ in the present paper are in good agreement with the data [6]. In addition, they match the results obtained for

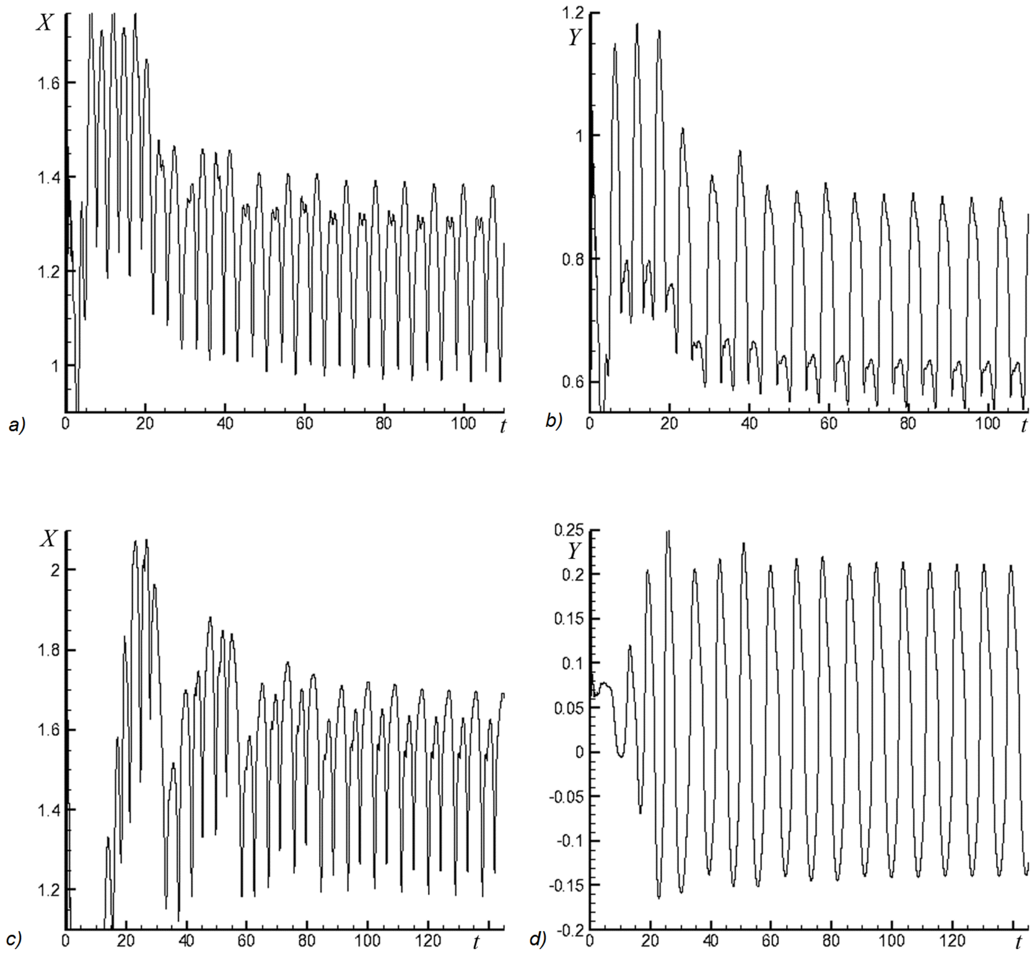

FIG. 2: (a) and (c) Behavior over time of the frontal *X* force acting on the NACA 0012 airfoil at a 60° angle of attack; (b) and (d) behavior over time of the lift *Y* force acting on the NACA 0012 airfoil at a 90° angle of attack

airfoil flow using the meshless technique of viscous vortex domains [19]. The obtained results show the limitation of the conclusion in Ref. [6].

Let us consider an airfoil under an angle of attack of 90°. This case differs slightly from the case of a normal-to-airstream plate. The experimental data [14] show that the drag coefficient is $C_D = 2.8$ for a plate of relative thickness equal to 0.2 at $\mathrm{Re} = 4 \times 10^4$. According to the data [20], the drag coefficient for a thin plate is $C_D \approx 2.5$. To compare the experimental data, a special testing problem of a flow over a normal-to-airstream thick plate was solved with the Reynolds number being equal to the experimental value. The numerical prediction was $C_D = 2.76$. Thus, the data misalignment of the airfoil drag at $\alpha = 90°$ in Ref. [6] cannot be explained by an inadequacy in the 2D URANS. Most

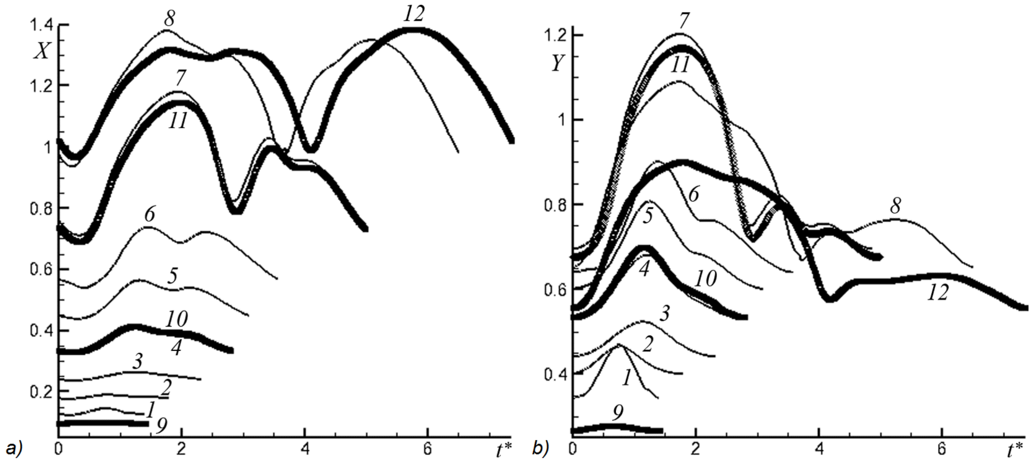

FIG. 3: Comparison of the reduced time t^* dependences of (a) longitudinal and (b) lateral loads on the airfoil at angles of attack from 15 up to 60° for computational domains with dimensions of 50 × 20 (curves 1–8 found using the Smirnov–Menter MSST modification) and 300 × 200 (curves 9–12): 1, α = 15°; 2, α = 20°; 3, α = 25°; 4, α = 30°; 5, α = 35°; 6, α = 40°; 7, α = 45°; 8, α = 55°; 9, α = 15°; 10, α = 30°; 11, α = 45°; 12, α = 60°

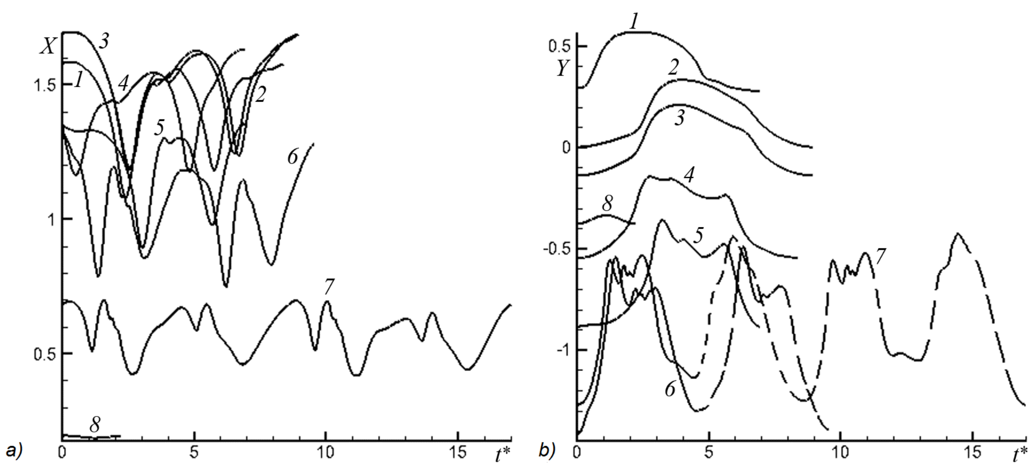

FIG. 4: Comparison of the reduced time t^* dependences of (a) longitudinal and (b) lateral loads on the airfoil at angles of attack from 75 up to 157.5°: 1, α = 75°; 2, α = 85°; 3, α = 90°; 4, α = 105°; 5, α = 120°; 6, α = 135°; 7, α = 150°; 8, α = 157.5°

likely, the reason for the considered misalignments is a difference in the 2D and spatial characters of the airfoil flow also observed in the physical experiments [4, 5, 14].

A more thorough comparison of the computational and estimated integral airfoil force loads in a moderate range of angles of attack is presented in Fig. 6. For small angles α

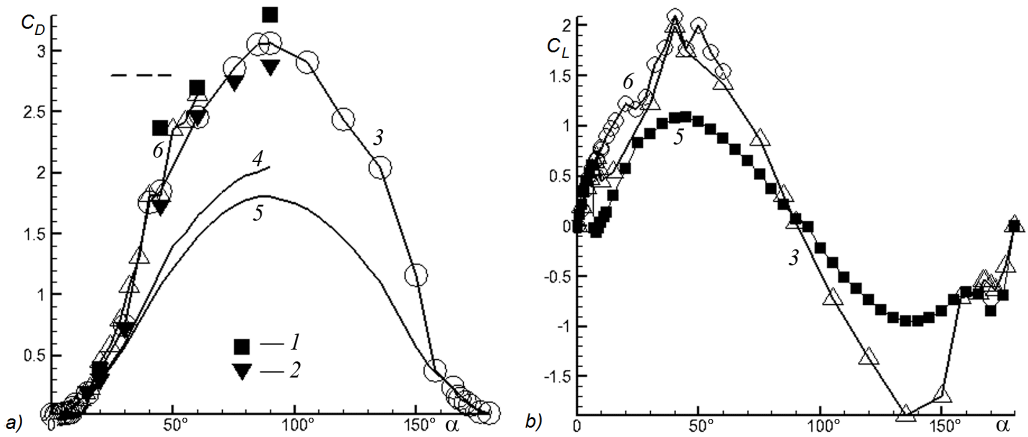

FIG. 5: Dependence of the angle of attack on the (a) drag coefficient and (b) lift coefficient averaged over a period of oscillations: 1, computation by URANS-MSST [3]; 2, computation by URANS-SA [3]; 3, computation by URANS-MSST (present work); 4, data from Ref. [10]; 5, data from Ref. [11]; 6, VVD method (dashed line, Ref. [4])

(up to 7–8°), the numerical predictions obtained with the grid and meshless techniques almost coincide with the estimated data [4]. This range of angles of attack corresponds to flow without separation over the NACA 0012 airfoil.

In the process of determining the parameters of airfoil flows without separation, some misalignments between the numerical predictions and their progressing deviations from the estimation data are observed. Although the dependences for $C_D(\alpha)$ are in good agreement for the grid and the meshless methods[1] [Fig. 6(a)] (and they obey the law close to quadratic one up to approximately 40°), the results of the computations of $C_L(\alpha)$ for moderate α (about 15–25°) demonstrate a difference in the representation of the spoon of the local decrease of C_L upon formation of the separation flow regime. The predictions using URANS for different computational domains are sufficiently close to each other.

For high angles of attack (close to 180°), the numerical predictions for C_D hardly differ from the estimated data [4], and the predictions for C_L, although they somehow differ from the data [4], represent a small spoon of C_L. The discrepancy of the results for $\alpha \leq 157.5°$ is most likely justification of the applicability of the 2D model in describing the considerable spatial flow over the airfoil.

The level of pulsating loads on the airfoil is sufficiently high (Fig. 7). If the pulsations of C_D reach 1 for a maximum value of C_D of about 3 (i.e., they are equal to approximately one-third), the pulsations of C_L reach 1.8 for the maximum absolute value of C_L, which is equal to 2 (i.e., they are of the same order). At the same time, the maximum pulsations of C_L correspond to the airfoil turning by a sharp end toward the incoming flow. A reduction in the C_L pulsations in the case where the airfoil position is

[1]The computation using the meshless VVD method [19] was performed by Ya. A. Dynnikov.

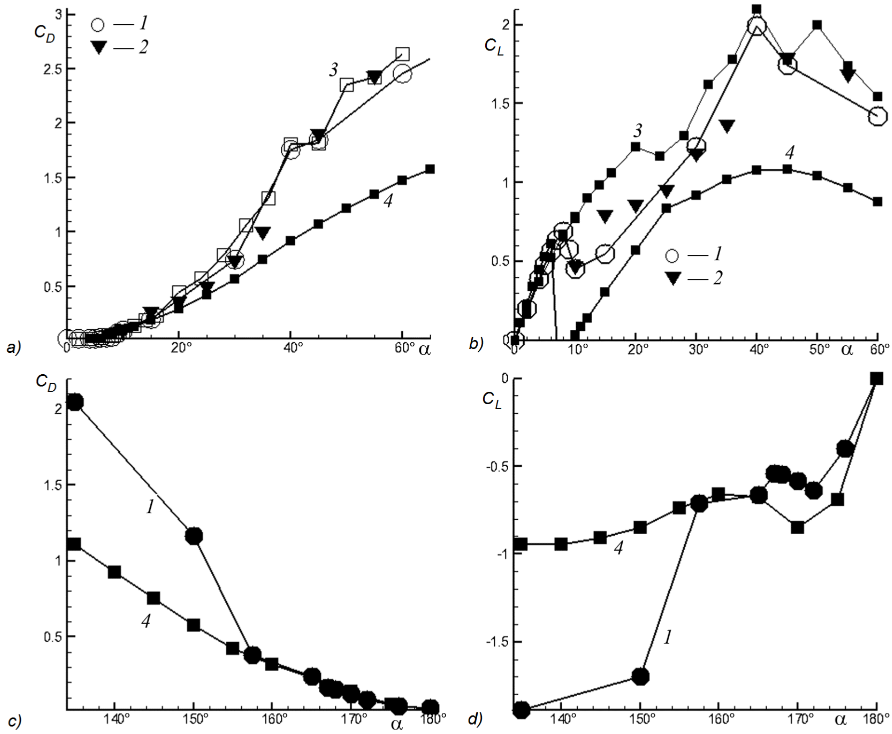

FIG. 6: Comparison of the dependences of the averaged over a period of oscillations for (a) and (c) $C_D(\alpha)$ and (b) and (d) $C_L(\alpha)$ on (a) and (b) moderate and (c) and (d) high angles of attack, obtained using URANS (1, for computational domains with dimensions 1, 300 × 200; 2, for computational domains with dimensions 50×20; 3, in the context of the VVD method; 4, with estimations) [11]

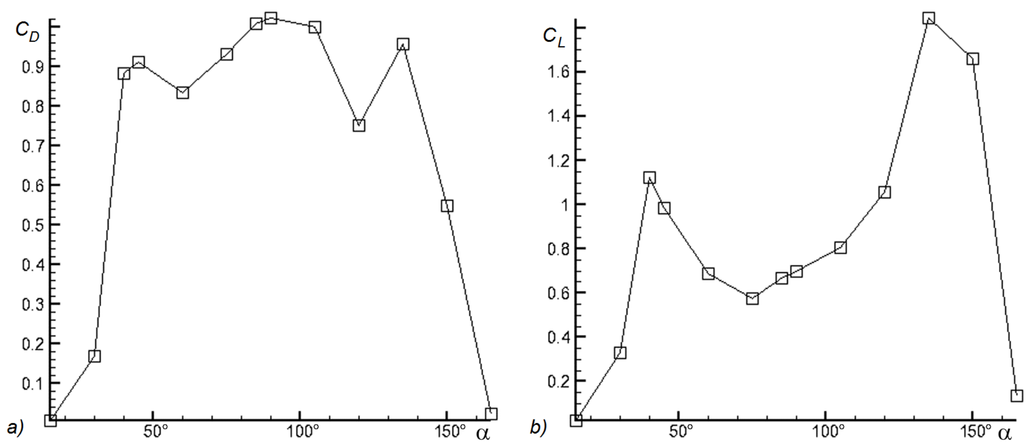

FIG. 7: Dependences of the pulsation (a) longitudinal and (b) lateral loads of the airfoil on the angle of attack

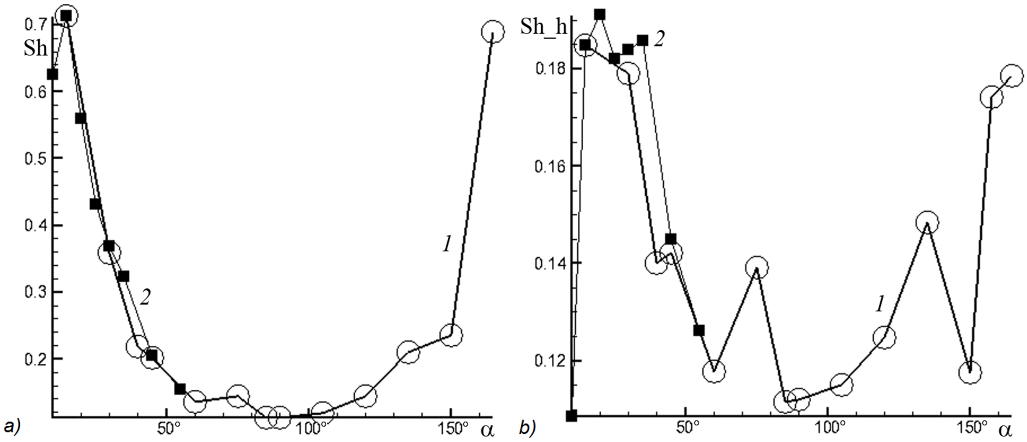

FIG. 8: Dependences of the (a) Strouhal number and (b) reduced Strouhal number on the angle of attack: 1, 300 × 200; *2*, 50 × 20

close to the normal one is related to the reduction in the airfoil chord projection onto the free-stream direction.

Processing the data by the periods of oscillations in Figs. 3 and 4 enables us to construct the dependences of the Strouhal number (Sh) determined by the chord on the angle of attack [Fig. 8(a)]. The predictions for the various-size computational domains are in satisfactory agreement. A considerable dispersion of Sh from 0.7 up to 0.1 seems to have a non-physical nature and is associated with the fact that the airfoil projection onto the normal direction to the flow is reduced as long as the angles of attack approach zero and 180°, correspondingly. The determination of the reduced Sh_h by a variable dimension (airfoil chord projection onto the perpendicular direction to the incoming flow) significantly reduces the range of Sh variation [from 0.11 to 0.19, see Fig. 8(b)]. Thus, the angle of attack significantly influences the character of the periodical oscillations in the wake because Sh at $\alpha = 90°$ is on the order of 0.1, which is more than twice lower than that for a circular cylinder. This is specified to a large extent by variation of the topology of the vortex structures in the far-field wake, which are analyzed subsequently.

5. ANALYSIS OF THE EVOLUTION OF THE VORTEX STRUCTURES AND LOCAL PARAMETERS IN NEAR- AND FAR-FIELD WAKES

Figure 9 compares the patterns of the vortex structures in a wake behind the airfoil at different time moments (see panels A, B, and C, where $t = 40$, 60, and 100, respectively) upon variations in wide ranges of the angle of attack (from 15 to 165°). The visualization of the structures is performed by vortex viscosity equal-value lines, with the number of the equal-value lines being fixed and equal to 21 for each of the calculated variants, and the maximum of the vortex viscosity being different.

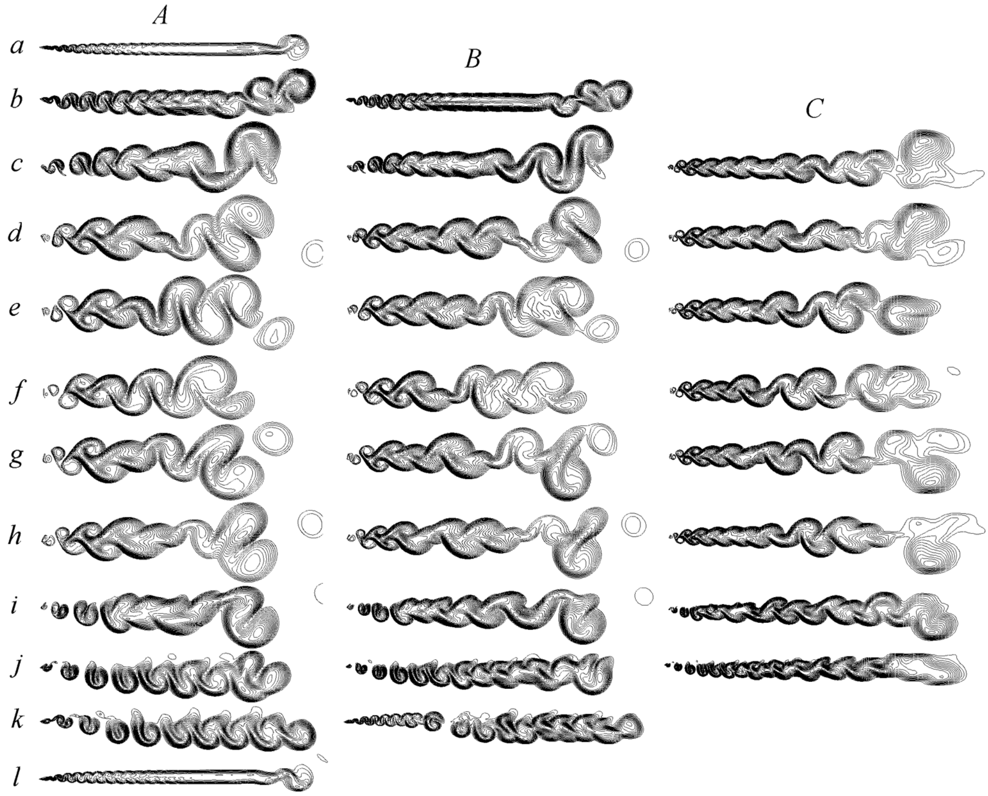

FIG. 9: Vortex viscosity patterns for α (A, $t = 40$; B, $t = 60$; C, $t = 100$): (a)–(j) from 15 to 150° with a step of 15°; (k) at 157.5°; (l) at 165°

A qualitative comparison of formed vortex trails by the shape of the generated vortices, their concentration, and extension is performed. As long as the airfoil integral parameters reach the regime of self-induced oscillations, the number of variants of the analyzed trails is reduced; that is, the range of variations of the angle of attack is reduced. At small and very high (close to 180°) angles of attack, reaching the regime of self-induced oscillations occurs in time moments of about 40 (Fig. 9, panel A); with the wake extension exceeding the whole extension of the vortex trails at angles of attack within a range of 60–120°.

A vortex trail behind the airfoil at small angles of attack (of approximately 15°) has a shape of coupled vortices of different orientations, generated at a periodical separation of the flow from the middle part of the airfoil contour and from its leading edge by turning [11]. As can be seen in Fig. 9 (panel A), at time moment $t = 40$ and $\alpha = 15$ and 165°, the vortex structure is arranged and uniform; the wavy boundary of the near-field wake gradually becomes smoother, and a vortex strip of constant width with a remaining starting vortex at the end (more precisely, what is left of the starting vortex by this time moment) is formed in the far-field wake. The regime of self-induced oscillations of the airfoil flow is reached considerably earlier than the indicated time moment. Note that the evolution of the vortex wake in the whole is not a periodical process.

When the angle of attack increases up to 30° a more intensive mixing in the wake is observed than that at small angles of attack (see Fig. 9). The coupling of vortices with different orientations with the formation of a strip trail of constant width (which becomes more and more extensive over time) occurs more prominently (Fig. 9, panels B and C). The fact that the starting vortex configuration is slightly varied in 20 units of dimensionless time from $t = 40$ to 60 attracts attention.

The airfoil arrangement at an angle of attack of 157.5° is accompanied by a turn of the sharp trailing edge toward the incoming flow. As a result, the trailing vortices at the initial time moments (approximately up to 30 units) are combined in separate vortex clusters (see Fig. 9). After that (see Fig. 9, panel C), a more arranged behavior of large-scale vortices is observed with the formation of the trail, similar to the case of an angle of attack at 30°.

The next group of vortex trails in the systematization corresponds to angles of attacks of 45, 135, and 150°. In the entire time range from 40 to 100 units, it is distinguished by the formation of isolated vortices in the process of their descent from the airfoil surface. In fact, these vortices are further combined in a trail with a strip tread form.

The final type of vortex trails corresponds to angles of attack from 60 to 120°. A sufficiently abrupt generation of vortices in the near-field wake is typical for them, which is accompanied by widening of the vortex trail. The topology of the trails is uniform and has the aforementioned strip protector form.

The patterned airfoil streamlines, averaged over a period of oscillations of lateral force (see Figs. 3 and 4) at various angles of attack for two scales are shown in Figs. 10 and 11. To some extent, they confirm the conclusions made from the analysis of unsteady vortex structures. Indeed, it is seen in Fig. 10 that the separation flows near the airfoil can be divided into the following groups: the first group corresponds to 30, 45, 135, and 150°; the second group corresponds to the range from 60 to 120°. For the first group, a small extension of the circulation zone in the wake is typical, with the formed large-scale vortices being adjacent to the airfoil. In the second group, multiple extensive zones of separation are formed behind the airfoil, which are propagating sufficiently far in the downstream direction.

The character of the large-scale vortices reattached to the airfoil is shown in more detail in Fig. 11. As long as the angle of attack increases, the vortex with the separation point in the vicinity of the smoothed leading edge, which initially covered the entire upper arc of the airfoil, starts to decrease; that is, the divergence point moves away from the sharp trailing edge. In this process, the longitudinal (along the airfoil) size of the vortex turns out to be lower than half the chord, except for an angle of attack of 90°, where this vortex is in fact absent; that is, it is part of the general vortex system. At the same time, the lateral size of the vortex remains approximately the same despite the fact that the vortex is submerged in the vortex wake at high angles of attack.

At $\alpha = 90°$, the structure of the vortex wake in the vicinity of the airfoil is symmetrical with respect to the central line that passes through the origin of the coordinates in the

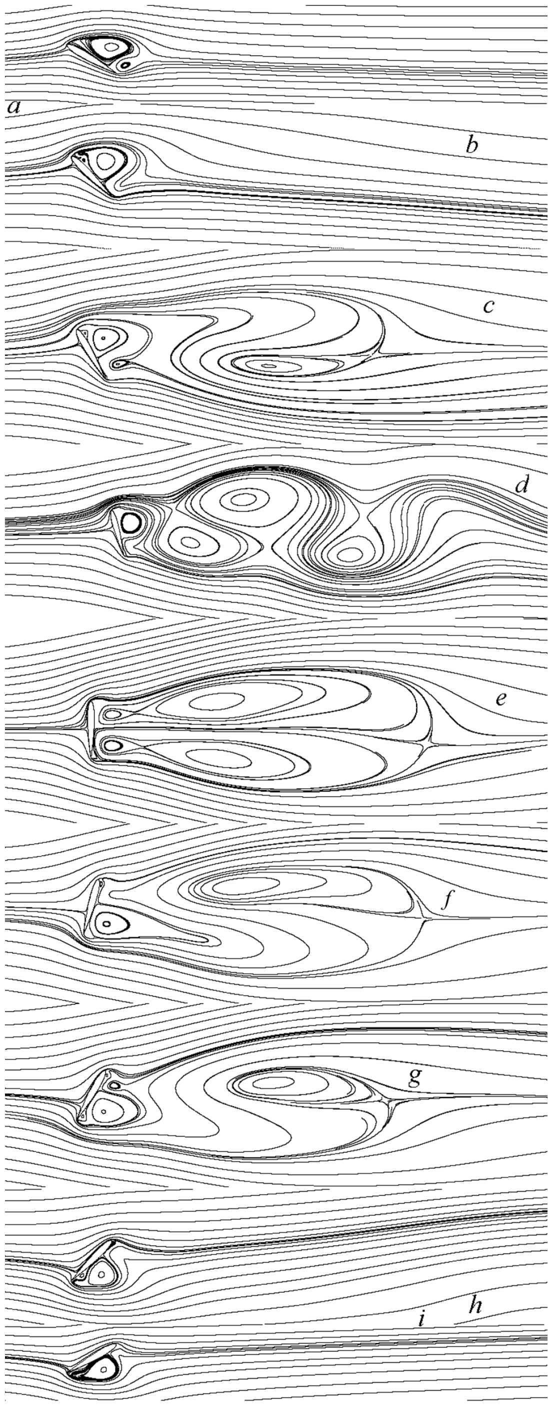

FIG. 10: (a)–(i) Averaged patterns of the flow over the airfoil from 30 to 150° with a step of 15°

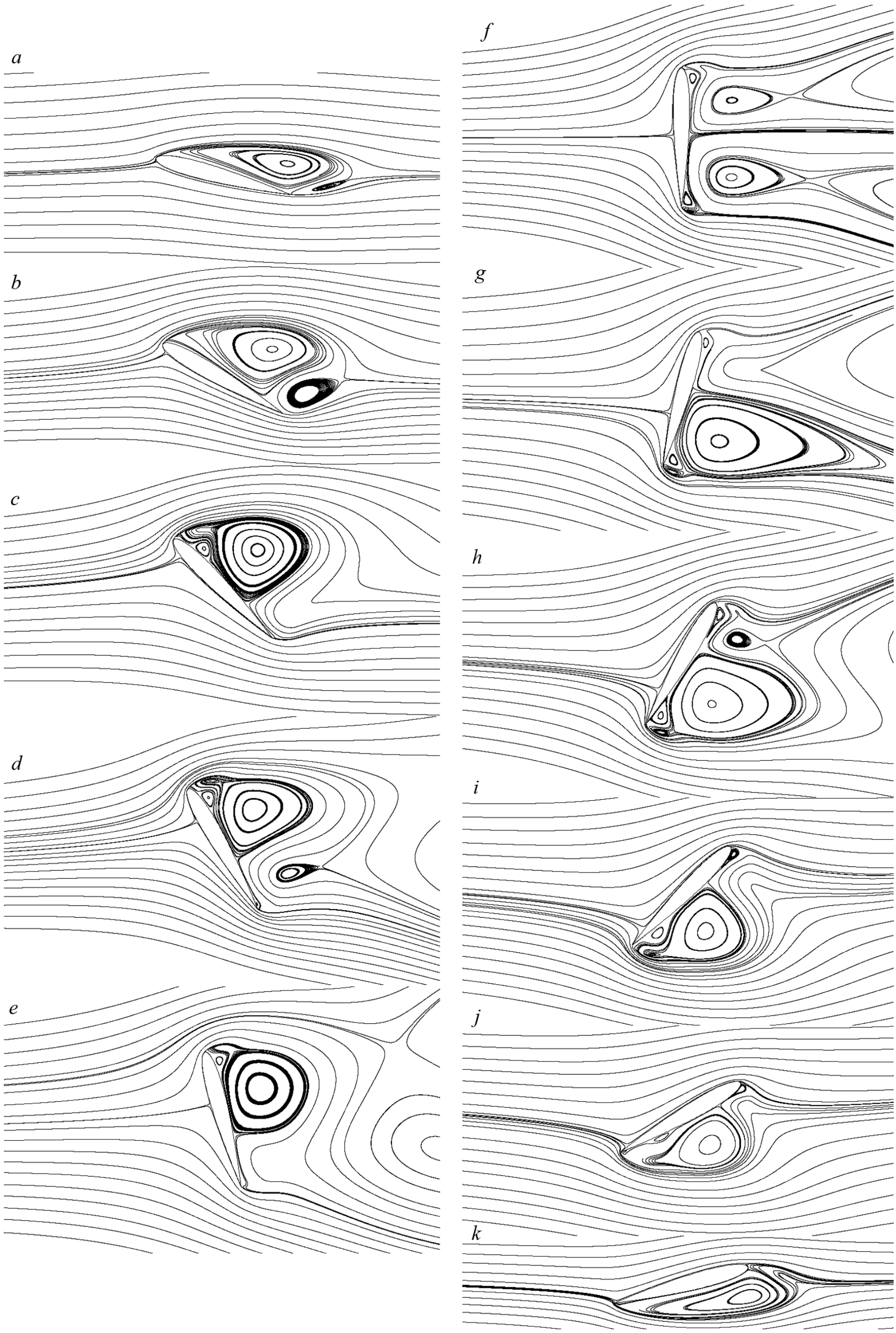

FIG. 11: (a)–(k) Streamlines averaged over a period of oscillations of C_L near the airfoil for the angles of attack from 15 to 165° with a step of 15°

airfoil middle. When the airfoil turns at its sharp edge toward the incoming flow, the reattached vortex with the separation point on the edge somehow initially increases its dimensions (the longitudinal size is longer than an airfoil half-chord, and the lateral size exceeds the chord). Then, as long as the angle of attack increases, it decreases. At α = 165°, the structure of the reattached vortex is approximately the same as at α = 150°. The generation of secondary small-scale vortices in the vicinity of the edges is observed at high angles of attack, and the generation of separation bubbles is observed at α = 135 and 150° [Figs. 11(i) and 11(j)].

The next group of the calculated data is, in general, methodological and is related to the analysis of the behavior of local parameters of the flow around the airfoil at an angle of attack of 90°. In this case, different turbulence models are applied in the computations, namely, the conventional MSST, MSST SM, and SA models.

The base pressure behind the airfoil at an angle of attack of 90° on a lateral force period of oscillations are varied in a sufficiently wide range, namely, from −3 to 0 (in the dimensionless form, this parameter has the meaning of a half-base pressure coefficient). When the process is averaged, the averaged pressure sufficiently and strongly decreases in the airfoil central part, reaching a level of −1.5, whereas the pressure near the edges increases up to −1.1 in the vicinity of the leading edge and −0.9 in the vicinity of the trailing sharp edge. The base pressure pulsations are high; they reach the minimum value of 0.9 in the central part and have two local minima (1.5 and 1.4) in the upper and lower parts of the airfoil upper arc. On the lower arc, directed toward the incoming flow, the maximum pulsations of pressure take place in the vicinity of the edges and reach 1–1.2.

As can be seen in Fig. 12, the vortex wake is split into the typical groups. The starting vortex, together with a system of random small cloddy vortices, is connected by a bridge with the next group, which resembles the first group by its random character. Then, after a transition layer, there is an arranged group of vortices of the protector form, which are likely to determine the self-induced oscillation regime of the airfoil integral parameters.

Figures 12(a)–12(c) show the vortex vorticity patterns in addition to the predictions by the Menter model. These patterns represent the vortex structures in a wake behind the airfoil at an angle of attack of 90°, obtained using the SA model. A considerably lower level (by 4 times) of the maximum viscosity, generated by the SA model, attracts attention. However, as shown in Figs. 12(d) and 12(e), the distributions of the integral force loads on the airfoil slightly differ. The arranged character of the vortex structures in Fig. 12(c) is maintained.

6. CONCLUSIONS

Based on the results from this study, the following conclusions can be drawn. First, the regime of self-induced oscillations of the time variation of the integral loads on the airfoil in a wide range of the angles of attack (from 15 to 165°) in the process of simulation within the context of solving the Reynolds-averaged Navier–Stokes equations using the multi-block computational techniques and semi-empirical turbulence models on extended

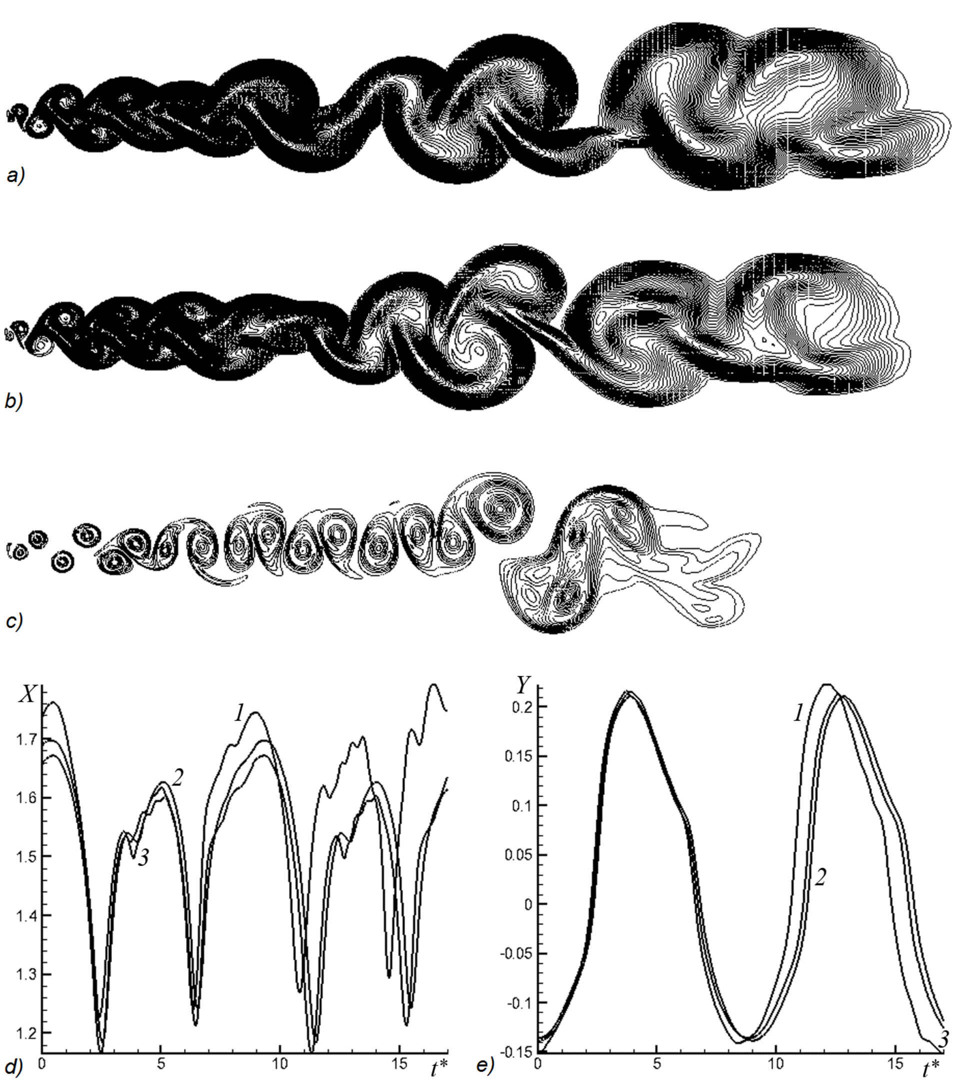

FIG. 12: Comparison of the vortex structures calculated by (a) MSST, (b) MSST SM, and (c) SA as well as of the distributions of (d) longitudinal and (e) lateral loads on the airfoil at $\alpha = 90°$: 1, MSST; 2, MSST SM; 3, SA (two periods of oscillations are shown, $t = 100$)

grids with resolution of the starting vortex in the computational domain is numerically validated. The periods of self-induced oscillations are determined by the extension of the periodical variation of the lateral force that acts on the airfoil.

Second, the applicability of the 2D approach to simulation of the vortex wake behind the airfoil is validated by the example of flow over a normal-to-airstream thick (0.2 chord) plate. The misalignment of the data on the airfoil drag at $\alpha = 90°$ in Ref. [6] is not justification for an inadequacy in the 2D URANS approach. Most likely, the reason for the misalignment is in the difference between the 2D and three-dimensional characters of the flow over the airfoil, which was also observed in physical experiments [4, 5, 14].

Third, the numerical investigation has shown that the predictions of the averaged integral and local loads on the airfoil found using the two-parametrical conventional MSST model [16], the modified MSST SM version of this model, and the one-parameter SA model of vortex viscosity in the URANS approach, as well as by solving the Navier–Stokes equations by the meshless method of vortex domains are in good agreement. The level of the maximum vortex viscosity in the wake in the case of the SA model is four times lower than that for the Menter model, including its modified version. Note that the reasons for this good agreement of the C_D predictions from the airfoil when solving the URANS equations using the grid method and the non-averaged Navier–Stokes equations using the meshless method require additional analysis.

Fourth, analysis of the evolution of vortex structures in the wake behind the airfoil at time moments 40, 60, and 100, as well as of the patterns of the separated flows over the airfoil, averaged over a period of oscillations of the lateral force, enables distinguishing two structural groups with generation of compact (at angles of attack of 30, 45, 135, and 150°) and extended (at angles of attack from 60 to 120°) circulation zones. The aforementioned groups are also divided by the behavior of the turbulent parameters, namely, the displacement of the maxima of the vortex viscosity at a considerable distance from the airfoil in the far-wake zone is typical for the first group, and the localization of the maximum of the energy of turbulence and vortex viscosity in the near wake is typical for the second group. In addition, it should be noted that a clearly distinguished region of variation of C_D pulsations corresponds to the second group.

Fifth, as was expected, the C_L predictions in the case of the flow without separation over the airfoil at small angles of attack (up to 7°) are in good agreement with the estimations [4, 5]. For the regimes of flows with separation and generation of separation bubbles and low-intensive circulation zones at angles of attack up to 20° and from 157.5 up to 180°, it was obtained that the computational results averaged over a period of self-induced oscillations and the estimated data [1] for C_D are in good agreement and those for C_L are in somewhat worse agreement. However, in this case, a spoon on the C_L curve is represented quantitatively and qualitatively. The reasons for the misalignment of the data are not sufficiently understood, which are possible related to an estimation ambiguity of the experimental unsteady loads.

Sixth, it was shown from the analysis of the averaged loads on the airfoil that the longitudinal force pulsations within a range of angles of attack from 40 to 135° were approximately 30% of the maximum load on the airfoil, and the maximum pulsations of the lateral force (at an angle of attack of 135°) were of the same order as the maximum lateral force that acted on the airfoil.

Finally, it was shown based on the analysis of the self-induced oscillations of the lateral force acting on the airfoil that the reduced Strouhal number determined from the chord projection onto the normal line to the free-stream velocity vector varied from 0.11 to 0. 14 within a range of angles of attack from 40 to 150°.

ACKNOWLEDGMENTS

This study was supported by the Russian Foundation for Basic Research (Projects Nos. 11-01-00039, 12-08-90001, and 12-01-00985) and by the Federal Targeted Program "Scientific and Scientific-Pedagogical Personnel of the Innovative Russia" (Grant No. 14.740.11.0880).

REFERENCES

1. Golovina, N. V., Comparison of the results of numerical calculations by the method based on the Godunov–Kolgan–Rodionov difference scheme with the experimental data for the transonic flow around RAE 2822, *TsAGI Sci. J.*, vol. **40**, no. 5, pp. 571–585, 2009.
2. Pylypenko, A. O., Polevoy, O. B., and Prykhodko, O. A., Numerical simulation of Mach number and angle of attack influence on regimes of transonic turbulent flows over airfoils, *TsAGI Sci. J.*, vol **43**, no. 1, pp. 1–36, 2012.
3. Bogatyrev, V. V. and Petrov, A. V., Numerical simulation of a spanwise jet blowing effect on a flow around a wing airfoil, *TsAGI Sci. J.*, vol. **43**, no. 2, pp. 137–145, 2012.
4. Hoerner, S. F., *Fluid-Dynamic Lift*, pp. 4–19, Bricktown, NJ: Hoerner Fluid Dynamics, 1975.
5. Sheldahl, R. E. and Klimas, P. C., Aerodynamic characteristics of seven symmetrical airfoil sections through 180-degree angle of vertical axis wind turbines, *Sandia National Laboratory Energy Report SAND80-2114*, 1981.
6. Garbaruk, A. V., Strelets, M. Kh., and Shur, M. L., Turbulence simulation in the calculations of complex flows, *Tutorial*, St. Petersburg, Russia: Izdanie Politekhnicheskogo Universiteta, 2012 (in Russian).
7. Isaev, S. A., Zhdanov, V. L., and Niemann, H.-J., Numerical study of the bleeding effect on the aerodynamic characteristics of a circular cylinder, *J. Wind Eng. Ind. Aerodyn.*, vol. **90**, no. 11, pp. 1217–1226, 2002.
8. Isaev, S. A., Baranov, P. A., Kudryavtsev, N. A., and Zhukova, Yu. V., Numerical simulation of unsteady heat transfer at a turbulent flow around a circular cylinder. Part 1. Methodic study, *Thermophys. Aeromech.*, vol. **12**, no. 1, pp. 27–39, 2005.
9. Isaev, S. A., Baranov, P. A., Kudryavtsev, N. A., and Zhukova, Yu. V., Numerical simulation of unsteady heat transfer at a turbulent flow past a circular cylinder. Part 2. Autooscillatory regime analysis, *Thermophys. Aeromech.*, vol. **12**, no. 2, pp. 271–283, 2005.
10. Isaev, S. A., Baranov, P. A., Kudryavtsev, N. A., Lysenko, D. A., and Usachov, A. E., Comparative analysis of the calculation data on an unsteady flow around a circular cylinder obtained using the VP2/3 and fluent packages and the Spalart–Allmaras and Menter turbulence models, *J. Eng. Phys. Thermophys.*, vol. **78**, no. 6, pp. 1199–1213, 2005.
11. Isaev, S. A., Soludakov, A. G., Baranov, P. A., Usachov, A. E., Strizhak, S. V., Lokhanskii, Ya. K., and Guvernyuk, S. V., Development, verification, and application of the open-type threaded software package VP2/3, based on multi-block computer technologies, to solve fundamental, applied, and exploitation problems in aeromechanics and thermophysics, *Mathematical Modeling and Programming Series*, Vestnik of the South Ural State University, vol. **17**, no. 3, pp. 59–72, 2009 (in Russian).

12. Ermishin, A. V. and Isaev, S. A., eds., *Control of the Flow Of Bodies with Vortical Cells When Applied to the Integral-Layout Aircraft (Numerical and Physical Modeling)*, Moscow: MGU, 2003 (in Russian).
13. Bystrov, Yu. A., Isaev, S. A., Kudryavtsev, N. A., and Leontiev, A. I., *Numerical Simulation of Vortex Intensification of Heat and Mass Transfer in a Bank of Tubes*, St. Petersburg, Russia: Sudostroenie, 2005 (in Russian).
14. Igarashi, T. and Terachi, N., Drag reduction of flat plate normal to airstream by flow control using a rod, *Proc. of 4th International Colloquium on Bluff Body Aerodynamics and Applications*, Expanded Abstracts, pp. 635–638, Bochum, Germany: Ruhr-University Bochum, 2000.
15. Fletcher, C. A. J., *Computational Techniques for Fluid Dynamics*, vol. **2**, Berlin: Springer, 1988.
16. Menter, F. R., Kuntz, M., and Langtry, R., Ten years of industrial experience with the SST turbulence model, *Turbulence, Heat and Mass Trans*fer, vol. **4**. K. Hanjalić, Y. Nagano, and M. Tummers, eds., pp. 625–632, Redding, CT: Begell House, 2003.
17. Smirnov, P. E. and Menter, F. R., Sensitization of the SST turbulence model to rotation and curvature by applying the Spalart–Shur correction term, *J. Turbomach*., vol. **131**, no. 4, pp. 041010-1–041010-8, 2009.
18. Spalart, P. R. and Allmaras, S. R., A one-equation turbulence model for aerodynamic flows, *AIAA Paper 92-0439*, 1992.
19. Andronov, P. R., Guvernyuk, S. V., and Dynnikova, G. Ya., Vortical Methods of Computation of Unsteady Hydrodynamic Loads, Moscow: Izdatelstvo MGU, 2006 (in Russian).
20. Leonard, B. P., A stable and accurate convective modeling procedure based on quadratic upstream interpolation, *Comput. Meth. Appl. Mech. Eng*., vol. **19**, no. 1, pp. 59–98, 1979.
21. Lien, F. S. and Leschziner, M. A., Approximation of turbulence convection in complex flows with a TVD-MUSCL scheme, *Proc. of 5th International Symposium on Refined Flow Modelling and Turbulence Measurements*, Paris, pp. 183–190, 1993.
22. Menter, F. R., Zonal two equation *k*-ω turbulence models for aerodynamic flows, *AIAA Paper 93-2906*, 1993.
23. Belotserkovsky, S. M. and Nisht, M. I., *Separated and Unseparated Ideal Fluid Flow about Thin Wings*, Moscow: Nauka, 1978 (in Russian).

Pavel Andreevich Baranov, Researcher, Battery Company "RIGEL"

Sergey Vladimirovich Guvernyuk, Candidate in Physical and Mathematical Sciences (Ph.D.), Deputy Director, Institute of Mechanics of the Lomonosov Moscow State University

Sergey Aleksandrovich Isaev, Doctor in Physical and Mathematical Sciences, Professor, Saint Petersburg State University of Civil Aviation

Aleksandr Grigoryevich Soudakov, Doctor in Technical Sciences, Chief Designer, Battery Company "RIGEL"

Aleksandr Evguenyevich Usachov, Candidate in Physical and Mathematical Sciences (Ph.D.), Leading Researcher, TsAGI